Electrostatic and Steric Contributions to Block of the Skeletal Muscle Sodium Channel by μ-Conotoxin

Kwokyin Hui,[1] Gregory Lipkind,[2] Harry A. Fozzard,[3] and Robert J. French[1]

[1]Department of Physiology and Biophysics, University of Calgary, Calgary, Alberta, Canada T2N 4N1
[2]Department of Biochemistry and Molecular Biology and [3]Department of Medicine, University of Chicago, Chicago, IL 60637

ABSTRACT Pore-blocking toxins are valuable probes of ion channels that underlie electrical signaling. To be effective inhibitors, they must show high affinity and specificity and prevent ion conduction. The 22-residue sea snail peptide, μ-conotoxin GIIIA, blocks the skeletal muscle sodium channel completely. Partially blocking peptides, derived by making single or paired amino acid substitutions in μ-conotoxin GIIIA, allow a novel analysis of blocking mechanisms. Replacement of one critical residue (Arg-13) yielded peptides that only partially blocked single-channel current. These derivatives, and others with simultaneous substitution of a second residue, were used to elucidate the structural basis of the toxin's blocking action. The charge at residue-13 was the most striking determinant. A positive charge was necessary, though not sufficient, for complete block. Blocking efficacy increased with increasing residue-13 side chain size, regardless of charge, suggesting a steric contribution to inhibition. Charges grouped on one side of the toxin molecule at positions 2, 12, and 14 had a weaker influence, whereas residue-16, on the opposite face of the toxin, was more influential. Most directly interpreted, the data suggest that one side of the toxin is masked by close apposition to a binding surface on the pore, whereas the other side, bearing Lys-16, is exposed to an aqueous cavity accessible to entering ions. Strong charge-dependent effects emanate from this toxin surface. In the native toxin, Arg-13 probably presents a strategically placed electrostatic barrier rather than effecting a complete steric occlusion of the pore. This differs from other well-described channel inhibitors such as the charybdotoxin family of potassium channel blockers and the sodium channel-blocking guanidinium toxins (tetrodotoxin and saxitoxin), which appear to occlude the narrow part of the pore.

KEY WORDS: single-channel conductance • lipid bilayers • peptide toxins • pore block • ion permeation

INTRODUCTION

Blocking toxins bind to the pores of ion channels and prevent ions from passing through. Charybdotoxin (Miller, 1995) and agitoxin-2 (MacKinnon et al., 1998) have been shown to dock as a cap over the potassium channel pore to inhibit ionic current. Tetrodotoxin and saxitoxin block at the selectivity filter (Hille, 1992) of a variety of sodium channels. μ-Conotoxin GIIIA (μCTX)* is a rigid, highly basic, 22–amino acid peptide toxin (see Fig. 1) which blocks voltage-gated sodium channels only from skeletal muscle (Gray et al., 1988). Although μCTX's solution structure is known (Fig. 1 A; Cruz et al., 1985) and its binding site overlaps with that of tetrodotoxin and saxitoxin (Moczydlowski et al., 1986), its mechanism of block is unclear. Block by a toxin involves two events: (1) binding to the channel and (2) inhibition of the ionic current. μCTX binding relies on multiple interactions with the channel, and is not absolutely dependent on any single toxin residue (Sato et al., 1991; Becker et al., 1992; Wakamatsu et al., 1992; Chahine et al., 1995, 1998; Dudley et al., 2000). In contrast, completeness of block of current by μCTX, depends critically on a single toxin residue, Arg-13 (Becker et al., 1992; French et al., 1996). Arg-13 of μCTX interacts strongly with the domain II residue Glu-758, which is located on the outer rim of the channel's outside vestibule (Chang et al., 1998). When this arginine is replaced by neutral glutamine, the bound mutant toxin allows a significant residual single-channel current (I_{res}), ~30% of the unblocked current (I_o; Becker et al., 1992). This and related partial blockers offer unique opportunities to study molecular determinants of ion channel function without mutating the channel protein (French et al., 1996; French and Horn, 1997). Here, we identify the electrostatic and steric requirements for μCTX block of the ionic current.

Address correspondence to Robert French, Department of Physiology and Biophysics, University of Calgary, 3330 Hospital Drive NW, Calgary, Alberta, Canada T2N 4N1. Fax: (403) 283-8731; E-mail: french@ucalgary.ca.

*Abbreviations used in this paper: μCTX, μ-conotoxin GIIIA; I_{res}, residual single-channel current with channel bound by toxin; F_{res}, fraction of control single-channel current remaining with channel bound by toxin.

MATERIALS AND METHODS

Peptide Synthesis

Peptide synthesis has been described in detail in Chang et al. (1998). In brief, linear peptides were produced by solid phase synthesis using 9-fluorenylmethoxycarbonyl (Fmoc) chemistry.

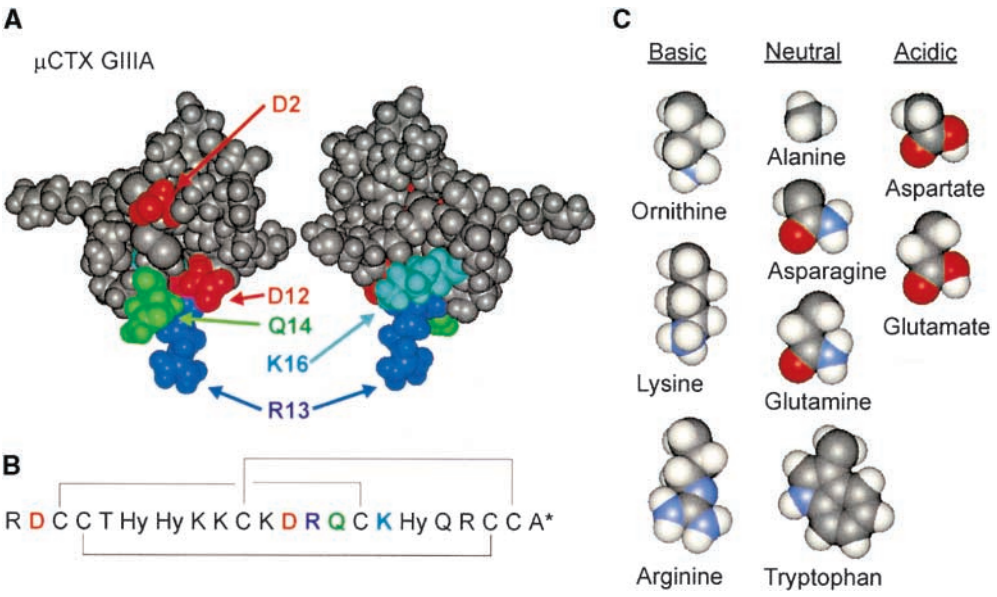

FIGURE 1. Structure of μCTX. (A) Aqueous solution tertiary structure of μCTX at pH 2. The two views differ by a rotation of ~180° around an axis defined by the R13 side chain, which is thought to enter the channel roughly parallel to the pore axis. Although the tertiary structure of μCTX is held rigidly by disulfide bonds, all charged residues point outwards from a discoidal structure of ~20-Å diameter and are likely flexible in solution. In this study, amino acid substitutions were made at positions 2, 12, 13, 14, and 16, as labeled. Coordinates from the Protein Data Bank (structure 1TCG; Lancelin et al., 1991). (B) Primary sequence of μCTX. μCTX is a 22–amino acid peptide toxin found naturally in the venom of the *Conus geographus* cone snail (Gray et al., 1988). The toxin contains seven basic (+) and two acidic (−) residues. With the amidated COOH-terminal (asterisk), nominal net charge of the toxin at neutral pH is +6. The structure is held rigid by three disulfide bonds (connecting brackets) between paired cysteine residues (Price-Carter et al., 1998; Kaerner and Rabenstein, 1999) and contains three modified amino acids, all hydroxyprolines (Hy; Gray et al., 1988). (C) Amino acid substitutions into position-13. Nominal side chain charge at pH 7 is indicated. Side chains are shown in space-filling representation, starting at C_α, without their backbone atoms.

Coupling of Fmoc amino acids was performed using the HBTU/HOBT/DIPEA method on a synthesizer (model 431A; Applied Biosystems). The raw peptides were air-oxidized and purified as previously described (Chang et al., 1998). During oxidation, cyclization was monitored by analytical HPLC and was usually complete after 2–3 d at 4°C. After folding of the peptide by air oxidation, toxin derivatives were purified to near homogeneity by HPLC (~95%, based on analytical HPLC). Active toxin derivatives were isolated as a single major peak. The identity of purified peptides were confirmed by quantitative amino acid analysis and, in some cases, by electrospray mass spectroscopy molecular weight determination.

As a check that the folded structures did not deviate qualitatively from that of the native toxin, for some derivatives 1-dimensional proton NMR spectra were recorded at 15°C in aqueous solution containing 5% D_2O at 500 MHz. The proton chemical shifts of the R13X derivatives were generally similar to those for the native toxin, with the exception of the shifts of Asp-12 and Gln-14, for which some change would be expected in response to substitution at the adjacent position 13. Qualitative NOE data indicate that the basic secondary structure remained the same in all cases tested. Others (Sato et al., 1991; Wakamatsu et al., 1992) also have reported that the R13A and R13K derivatives fold normally.

Membrane Vesicle Preparation and Bilayer Setup

Sodium channel-containing plasmalemmal vesicles were isolated as described before (Becker et al., 1992), sonicated, and incubated with 50 μM batrachotoxin (BTX) in a 0.3-M sucrose, 20-mM HEPES solution, pH 7.4, and kept at −20°C for at least 1 d before use to inhibit channel inactivation (Khodorov, 1985). 1–5 μl of incubated vesicles was pipetted into one well of a bilayer chamber containing a bathing solution of 200 mM NaCl (BHD), 10 mM MOPS (Sigma-Aldrich), 0.1 mM Na_2EDTA (Sigma-Aldrich), pH 7.0 (NaOH; BHD) in both wells. Bilayers were formed from a 4:1 mixture of phosphatidylethanolamine and phosphatidylcholine (Avanti Polar-Lipids) solution dissolved in decane (Fisher Scientific) before vesicle injection. Saturated 3-M KCl salt bridges linked the bathing solutions in each well to a 3-M KCl reservoir with which contact was made via Ag/AgCl electrodes.

Data Acquisition

After incorporation, channel orientation was determined from its voltage dependence of gating. Current measurements were taken with an Axopatch-1B patch amplifier (Bessel filtered at 5 kHz, 80dB/decade; Axon Instruments), digitized with a Neuro Data digitizer (model DR-384; Instruments Corp.), 8-pole low-pass Bessel filtered at 200 Hz (−3dB; model 902LPF; Frequency Devices), monitored on a digital oscilloscope (model 2090-IIIA; Nicolet Instrument), and recorded onto videotape (model AG-2200; Panasonic). Data were transcribed onto a computer during the recording or through the videotape, sampled at 1 kHz (Fetchex 5.5.1; Axon Instruments, Inc.).

Data Analysis

Data were analyzed by determining the single-channel amplitude directly from the current traces (Fetchan 6.04; Axon Instruments, Inc.). Records taken in the absence of conotoxin were used to distinguish between partially blocked, toxin-bound events (I_{res}) and open-channel (I_o) events. The fractional residual current is defined as $F_{res} = I_{res}/I_o$. Because of the voltage dependence of I_{res}, $F_{res}(0\ mV)$, determined by linear interpolation, was used to describe the degree of current block (see RESULTS and Fig. 2, B and C). For each experiment, the voltage was corrected for the net junction potential offset using the apparent reversal potential determined under symmetric ionic conditions. In all but four experiments, offsets were <5 mV. In I-E plots, data from multiple experiments were combined in voltage bins 5 mV in width. For the four experiments with offsets >5 mV, after offset correction, the current values were in agreement with the other experiments.

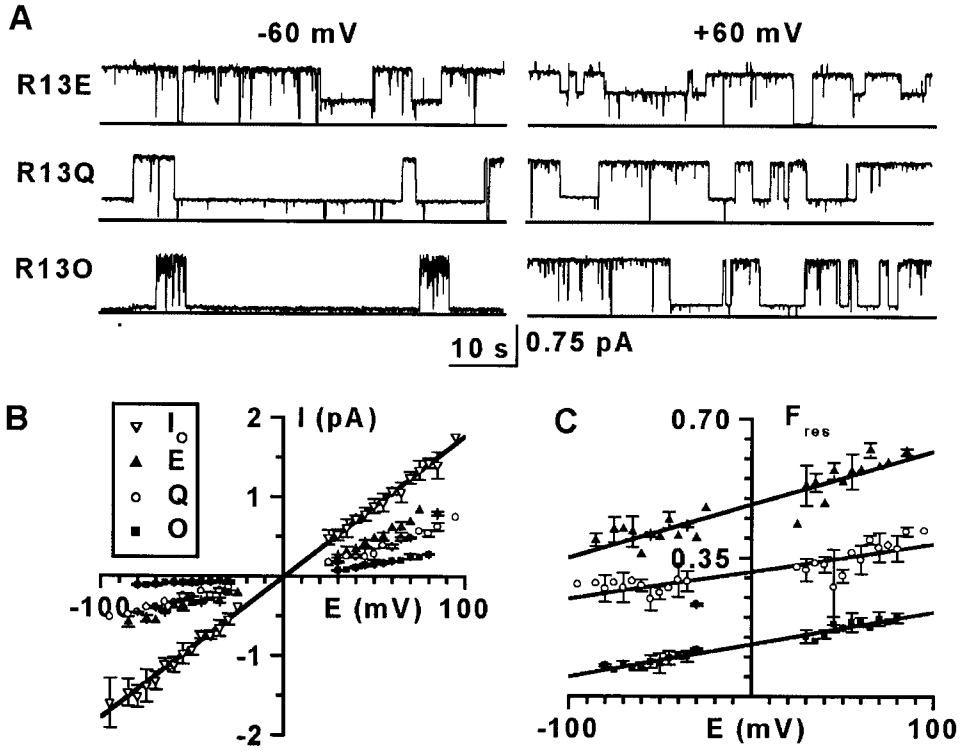

FIGURE 2. μCTX block of sodium channel current depends on toxin residue-13 charge, and the residual current shows outward rectification. (A) Single sodium channel current traces in the presence of three size-similar μCTX mutants, 100 μM R13E, 10 μM R13Q, and 4 μM R13O (ornithine-13), at +60 mV and −60 mV from one experiment for each mutant. Solid line at bottom of traces is 0-pA current. Large deflections away from the solid line (~1 pA) are channel openings. Intermediate deflections represent current through the open channel, when bound by a toxin mutant (residual current). (B) Current-voltage plots of R13E, R13Q, and R13O averaged from six, five, and four experiments, respectively. I_o, the unblocked single channel current, is averaged from the lumped R13E, R13Q, and R13O experiments ($n = 15$). As previously observed, at extreme voltages (beyond ±50 mV) the current-voltage plot of I_o deviates slightly from linearity (Ravindran et al., 1992); however, the I_{res} plots of the residual currents for toxin mutant blocking events deviate significantly from linearity even at low voltages. (C) Fractional residual current of R13E, R13Q, and R13O from part B. $F_{res} = I_{res}/I_o$. A linear fit was used to determine $F_{res}(0\ mV)$. The standard error in the fit of $F_{res}(0\ mV)$ was used as the error in plots of $F_{res}(0\ mV)$.

Molecular Modeling and Electrostatic Calculations

The Na channel outer vestibule was modeled as previously described (Lipkind and Fozzard, 2000). Briefly, the pore-lining P loops of the Na channel were modeled as an α-helix-turn-β-strand motif, which preserves the relationships required for channel interactions with tetrodotoxin and saxitoxin that have been found experimentally. The outer vestibule was completed by docking the P loops of domains I-IV into the extracellular part of the inverted teepee structure, formed by the S5 and S6 α-helices, that were spatially located by homology modeling based on the backbone coordinates of the KcsA potassium channel (Doyle et al., 1998)

Electrostatic difference potentials ($\Delta\varphi$) were calculated inside the model of the sodium channel outer vestibule, containing a docked conotoxin (Chang et al., 1998), using the DelPhi module of Insight II (MSI, Inc.). The DelPhi module calculates the electrostatic potentials in and around molecules using a finite difference solution to the nonlinear Poisson-Boltzmann equation (Gilson and Honig, 1987; Sharp and Honig, 1990). The dielectric constants were set to 10 for the protein interior (for review see Antosiewicz et al., 1994) and 80 for the solvent water region. The carboxylates groups of Glu and Asp, the amino group of Lys, and the guanidinium group of Arg were assumed to be unit charges. The difference potentials are given with respect to the potential in the complex of the WT toxin docked in the pore (see Figs. 5 and 6 B and Tables I and II) or with respect to the complex of R13Q with the channel (Table II). For doubly substituted derivatives (R13Q/XnY), difference potentials were initially calculated with respect to the R13Q complex, and then expressed with respect to the WT complex by addition of $\Delta\varphi$(R13Q-WT). Difference potentials are given in units of kT/e, where k is Boltzmann's constant, T is temperature in degrees Kelvin, and e represents the elementary positive charge.

RESULTS

Residue-13 Charge Is a Critical Determinant of Block

We measured currents through single, batrachotoxin-activated channels, in the presence and absence of various μCTX derivatives. R13Q was the only point mutant of μCTX previously found to allow an $I_{res} > 0$ (Becker et al., 1992). Residue-13 is known to interact, at least electrostatically, with several residues along the permeation pathway (Dudley et al., 1995; Chang et al., 1998), especially Glu-758 (interaction energy interaction energy −2.5 kcal/mol), a residue important for high sodium conductance (Terlau et al., 1991; Chiamvimonvat et al., 1996a,b). In Fig. 2, we compare the fractional residual current at 0 mV ($F_{res}(0\ mV)$; see MATERIALS AND METHODS) for three R13X derivatives of μCTX with different residue-13 charges but similar size: R13E, R13Q, and R13O (ornithine-13; see Fig. 1 C for all residue-13 substitutions). These charge-changing substitutions show residue-13 charge to be critical for current block. In comparison to R13Q, a negative substitution (R13E) enhanced $F_{res}(0\ mV)$, whereas a positive one (R13O) reduced it (Fig. 2 C). The results suggest a strong electrostatic contribution to current block by μCTX.

Residue-13 Size Affects Block

Residue-13's binding interaction with Glu-758 on the

channel is not only electrostatic (Chang et al., 1998), suggesting that its influence on conduction also may involve other factors. To test whether residue-13 can sterically inhibit the current, we substituted residue-13 with amino acids of variable length and volume (e.g., glutamine in Fig. 2 A, asparagine and tryptophan in Fig. 3 A, and alanine were used as neutral substitutions of different sizes). With the substitutions grouped by their nominal elementary charge, F_{res}(0 mV) showed a similar dependence on residue-13 length within each group (Fig. 3 B), as reflected in the "steric attenuation" for each charge group (Fig. 3 C). Shorter residue-13 length resulted in lesser block. A comparable correlation was seen when side chain volume, instead of length, was used as an index of side chain size. The only exception to this pattern was R13A, which showed a smaller F_{res}(0 mV) than expected for its size, based on the data for the other substitutions. In general, decreases in residue-13 length allow an increased residual current, but there may be no further increase when the substituent is made sufficiently small.

Other Charges can Contribute to Block

Regardless of the size or charge of the residue-13 substituent, I_{res} shows outward rectification (Fig. 2, A and B, and Fig. 3 A), i.e., inward current is smaller than outward for equal and opposite driving voltages under symmetric ionic conditions. This contrasts with the linear I-V relation for the unblocked channel, and suggests that, in addition to residue-13, other toxin residues interact with ions that enter the channel. To determine the extent of contribution by other residues, we constructed several double mutants, based on the partial blocker (R13Q), with additional charge changes at positions 2, 12, 14, or 16. At first glance, charge changes at positions 2, 12, and 14 showed little influence on I_{res} (compare R13Q [Fig. 2 A] with D12N/R13Q and R13Q/Q14R [Fig. 4 A]). However, systematic examination of F_{res}(0 mV) shows that charge-changing substitutions near residue-13 (positions 12 and 14) have a greater effect on block than more distant substitutions (e.g., position 2; Fig. 4 B). The importance of each position was quantified by defining an "electrostatic attenuation" as stated in the figure legend (Fig. 4 C). This analysis also suggests that residue-16 charge has a more dramatic influence than residues 2, 12, or 14 (see *Modeling Electrostatic Effects*). These results reveal two important points about current block by μCTX: (1) the position of a charge on the toxin is an important determinant of its contribution to block; and (2) block by residue-13 can mask the effects of other toxin residues (individual neutralizations of neither residue-2, 12, nor 16, allowed any residual current; Becker et al., 1992).

Modeling Electrostatic Effects

The prominent role of charge in the magnitude of partial block implies a possible role for electrostatic exclu-

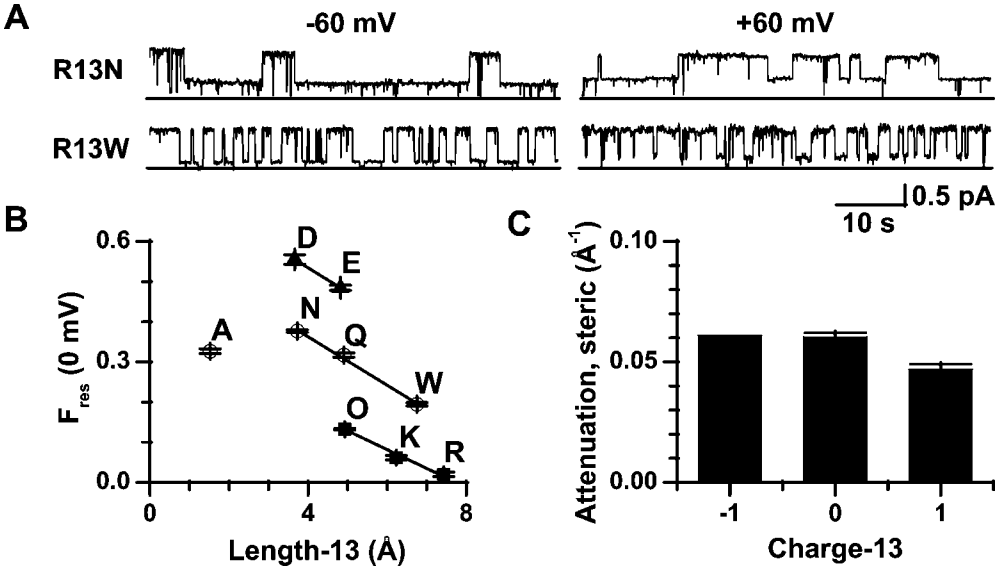

FIGURE 3. Single-channel current block by μCTX derivatives depends on toxin residue-13 length. (A) Single sodium channel current traces in the presence of μCTX mutants with a neutral residue-13: 10.5 μM R13N or 25 μM R13W, at +60 mV and at −60 mV from one experiment for each mutant. As with the charge-substitution mutants, the residual currents for residue-13 size-changing mutants show outward rectification. General features of traces are as described in Fig. 2 A. (B) In all charge-conservative substitution groups, F_{res}(0 mV) is linearly dependent on the length of the substitution >3.7 Å. The R13A mutant shows an F_{res}(0 mV) almost identical to R13Q, but smaller than R13N (see DISCUSSION). Data averaged from five, six, eight, four, five, four, four, seven, and four experiments for R13D, R13E, R13A, R13N, R13Q, R13W, R13O, R13K, and R13R (wild type), respectively. Length was determined in Chem3D (Cambridge Soft) as the distance between the centers of C_α and the most distant heavy atom in the stretched out form of the amino acid side chain. (C) The steric attenuation of single-channel current, defined as the slope of the plot of F_{res}(0 mV) versus length-13 (B), for all charge-conservative substitution groups >3.7 Å is nearly identical at approximately -0.05 $Å^{-1}$, summarizing the effect of length, independent of the influence of charge.

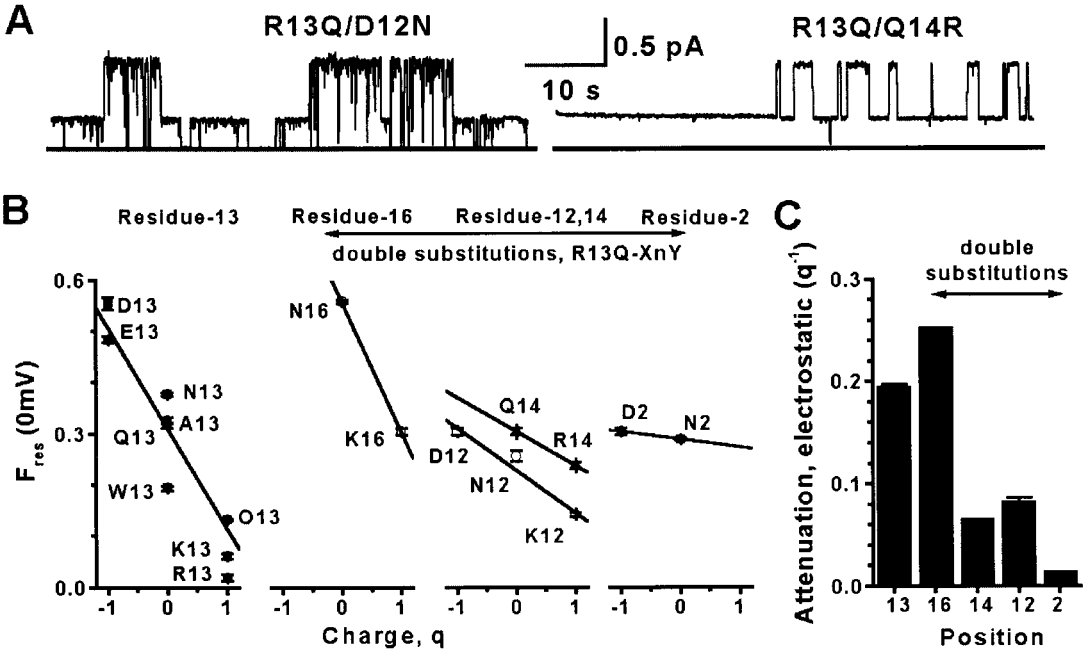

FIGURE 4. μCTX block of single-channel current is influenced by charges on the toxin. Data are shown for single substitutions of Arg-13 or for double mutants in which substitution of one of the residues Asp-2, Asp-12, Gln-14, or Lys-16 is paired with the R13Q substitution to give a measurable residual current. (A) Single sodium channel current traces in the presence of double mutants at +60 mV: 4 μM D12N/R13Q or 5 μM R13Q/Q14R. General features of traces are as described in Fig. 2 A. (B) Plot of F_{res}(0 mV) at five toxin positions (2, 12, 13, 14, and 16) shows that the greatest effect occurs with charge-changes at positions 13 and 16. The scatter, at each charge, in the residue-13 plot reflects the length dependence described in Fig. 3. Data averaged from multiple experiments, as described in Fig. 3 B for residue-13 substitutions, and from four experiments for each double mutant. Charge is defined as the nominal number of elementary charges at neutral pH on the amino acid at the toxin position of interest. (C) A plot of the electrostatic attenuation, defined as the slope of the linear fits from B, shows that the strongest attenuation of the current is induced by residues 13 and 16. Attenuation falls off with distance from these residues (also see Fig. 6 A).

sion as a mechanism for block. In Fig. 5, we show a molecular model of the pore vestibule–lining residues of the channel (Lipkind and Fozzard, 2000; see also Lipkind and Fozzard, 1994; Chang et al., 1998; Dudley et al., 2000), with μCTX held rigidly in place by the interactions of several toxin residues. The outer vestibule is thought to be a truncated funnel with a volume of ~300–400 A^3, large enough for 30–40 water molecules. In the model, Arg-13 intrudes into the outer vestibule and binds to its rim, but it does not sterically occlude the path leading to the selectivity filter. Instead, its positive charge energetically induces a "cation-excluded" volume that fills the narrow part of the pore, thereby preventing sodium permeation.

To explore the of role residue-13 charge in block of single-channel current, we calculated the change in electrostatic potential inside of the pore in the cases of substitution of Arg-13 by Lys, Gln, or Glu, with respect to the potential in the presence of Arg-13. Electrostatic difference potentials ($\Delta\varphi$) were calculated inside the model of the sodium channel outer vestibule, composed of the P loops and the S5 and S6 transmembrane helices of domains I–IV (MATERIALS AND METHODS). The difference potential calculation avoids the much more problematic estimation of absolute potentials and focuses the modeling on the experimentally defined differences among different toxin derivatives.

For substitution of Arg by Lys, the electrostatic potential became relatively more negative in the vicinity of the carboxylate group of the side chain of Glu-758 ($\Delta\varphi \sim -1$kT; Fig. 5 A). The shorter side chain of lysine interacts more weakly with Glu-758 than Arg-13, yielding a relatively negative potential in the vicinity and an associated increase of residual current. Neutralization or charge reversal at residue-13 produces a more dramatic effect. The R13Q substitution abolishes electrostatic screening of the negative charge of Glu-758, creating a strongly negative potential nearby (Fig. 5 B, see the −4.5kT contour). The surface corresponding to $\Delta\varphi = -1.0$kT almost fills the lumen of the outer vestibule. A further drop in $\Delta\varphi$ occurs when Glu is placed in position 13 (Fig. 5 C). Thus, the observed increase in residual current correlates well with the increasingly negative potential within the pore and with the decrease in the electrostatic neutralization by residue-13 of the negative electrostatic field generated by the carboxylate of Glu-758.

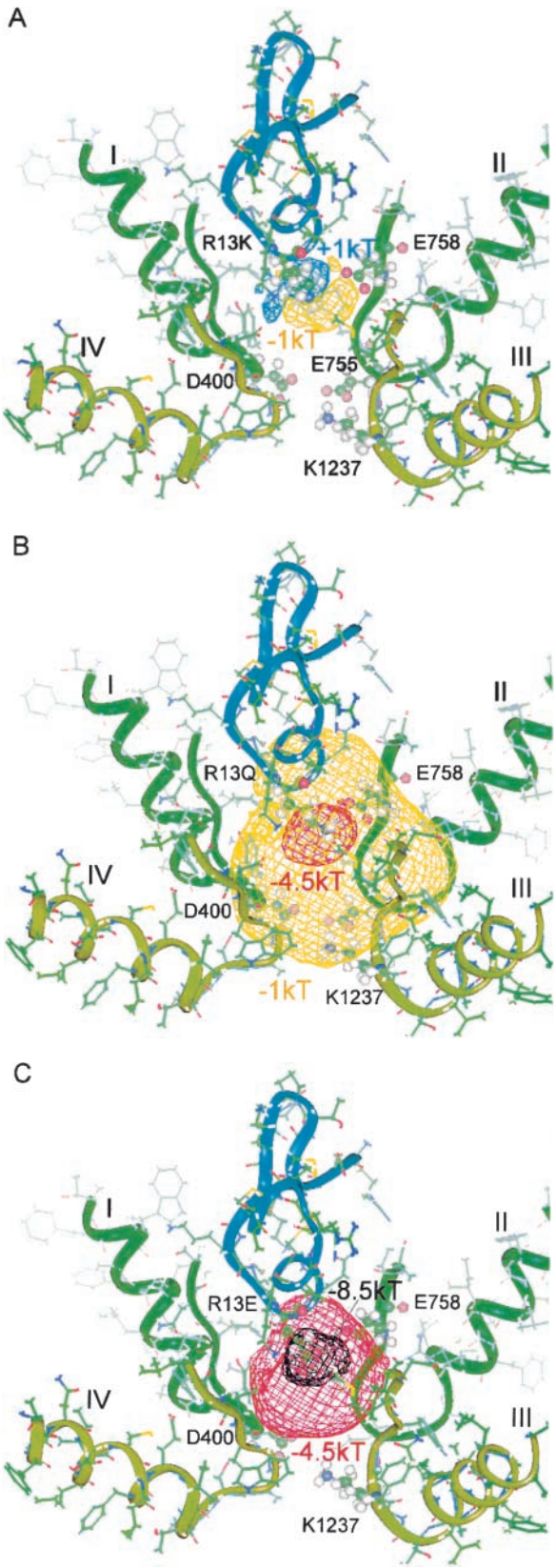

FIGURE 5. Electrostatic difference potential surfaces, calculated for the model of Lipkind and Fozzard (2000), showing an increase in a "permissive volume," which favors cation entry after Arg-13 substitutions. The different isopotential surfaces are shown as φ_{X13}–φ_{R13}. The surfaces, referenced to the wild-type toxin (Arg-13), are displayed for (A) R13K, (B) the archetypal partial blocker, R13Q, and (C) for R13E. For convenience, two different criteria levels are shown in each panel, where the more negative contour corresponds to the difference potential at Glu-758 for the mutant shown and the less negative one is equal to the deeper potential contour from the previous panel. The S5 and S6 helices from each domain were included in the calculations, but, for clarity, are not shown in the figure. The backbone of μCTX is shown in blue, and the backbones for the channel P-loops are shown in green and light green. Residue-13 of the toxin, Glu-758 of channel domain II, and the selectivity filter residues are shown as ball and stick representations.

TABLE I

Residual Currents and Calculated Difference Potentials at the Selectivity Filter for Substitutions at Residue-13 of μCTX

Substitution	Δφ (kT/e, at C_β of A1529) relative to WT toxin	F_{res} (0 mV)
R13K	−0.1	0.05
R13Q	−1.0	0.30
R13E	−1.8	0.48

As shown by these difference potential surfaces, substitution of neutral or acidic residues into position-13 allows a progressively larger fraction of the channel vestibule to be more easily cation-accessible, and consequently, ions pass through more freely. If we assume that sodium must reach the selectivity filter to permeate, then it is instructive to compare changes in electrostatic potential at the methyl group of Ala-1529, a member of the DEKA selectivity motif. Ala was chosen because it remains fixed in location, whereas the side chains of the other residues may be displaced by changes in nearby charges or field. Table I shows the difference potentials resulting from Arg-13 substitutions and their ordered relation to F_{res}(0mV). Shorter basic residues induce a smaller excluded volume than Arg-13, and their charges are sufficiently distant from the narrowest part of the pore that they do not block completely. Fig. 5 also suggests that Arg-13 can attenuate the normal catalytic influence of Glu-758 on cation permeation. Thus, the model offers two possible electrostatic mechanisms by which μCTX Arg-13 can block ion permeation: (1) the basic residue induces a cation-excluded volume, extending beyond its van der Waals volume, that interrupts the conduction pathway; and (2) Arg-13 masks the negative electrostatic field produced by Glu-758 in the vestibule, thereby reducing its normal enhancement of ion conduction.

The calculations shown in Table I and Fig. 5 are intuitively satisfying, but not surprising, as similar predictions might be made for various models in which Arg-13 was critical for block. However, coupling studies (Chang et al., 1998; Li et al., 2001b) indicate that μCTX interacts most intimately with domain 2 of the channel. Toxin residues that interact with this receptor

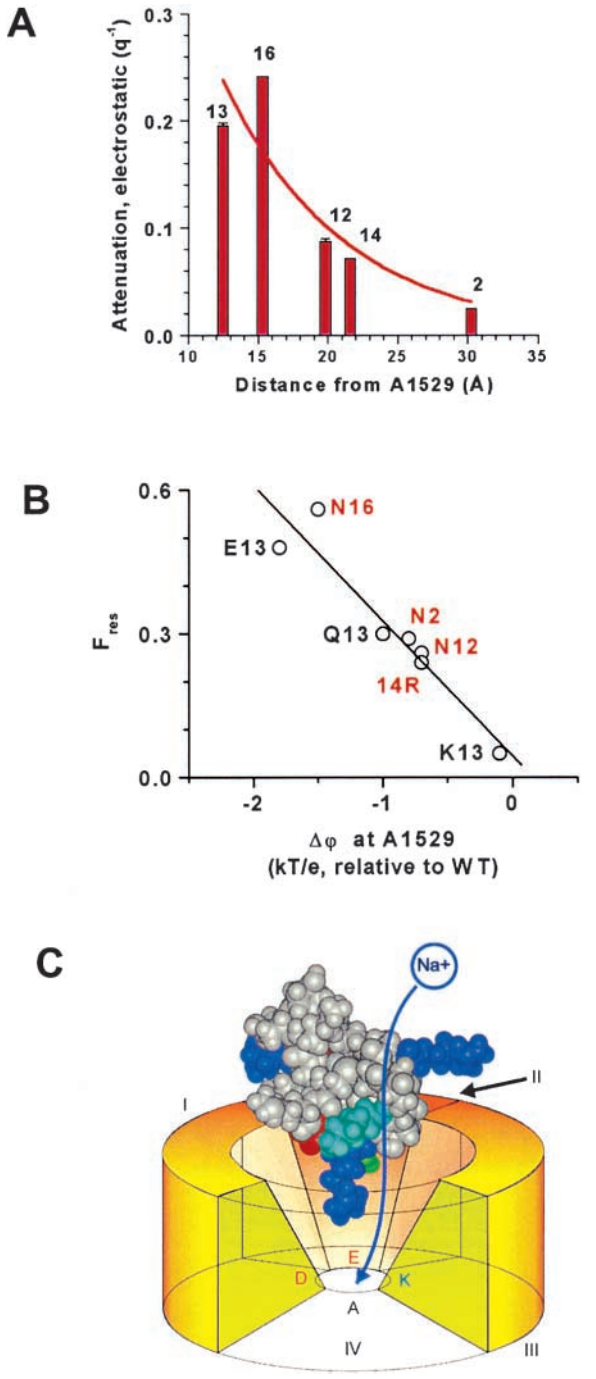

FIGURE 6. (A) The electrostatic attenuation of single-channel current (Fig. 4, B and C) decreases with distance of the charge change from the selectivity filter residue, Ala-1529. Coincidentally, the length constant for the decay of the attenuation (8.2 Å) approximately matches the Debye length in the bathing solution, indicating that the shielding within the vestibule of the toxin–pore complex is roughly equivalent to that in free solution. Extrapolation, to zero, of the smooth curve through the data points (arbitrarily drawn as an exponential) suggests that a single positive charge at Ala-1529 would be adequate to completely block current flow. (B) F_{res} is closely correlated with $\Delta\varphi$ estimated at C_β of Ala-1529 ($r = 0.95$, $P \approx 0.01$). Labeling is as in Fig. 4 B; double substitutions are labeled in red. (C) Cartoon of the model showing the putative path of ion flow through the partially occluded channel. The orientation of μCTX is similar to the right hand view in Fig. 1. On the toxin, arginine residues are shown in dark blue (Arg-1, top left; Arg-13, bottom; Arg-19 – top right); Lys-16, cyan; Asp-12, red; and Gln-14, green. The selectivity filter is made up of the DEKA residues from P loops of domains I-IV, respectively. Toxin residue Lys-16 faces the conducting path, consistent with its strong effect on the residual current. Arg-13 is nearest the DEKA ring.

TABLE II

Residual Currents and Calculated Difference Potentials at the Selectivity Filter for Doubly Substituted μCTX Derivatives of Form R13Q/XnY

Second substitution	Δφ (kT/e, at C_β of A1529) relative to R13Q	Δφ (kT/e, at C_β of A1529) relative to WT toxin	F_{res} (0 mV)
D2N (−/o)	0.2	−0.8	0.29
D12N (−/o)	0.3	−0.7	0.26
Q14R (o/+)	0.3	−0.7	0.24
K16N (+/o)	−0.5	−1.5	0.56

surface would be shielded from the conduction pathway by the bulk of the toxin. This prompted our experiments with R13Q/K16N, and the additional analysis shown in Fig. 6 (A and B) and Table II. Fig. 6 A shows empirically that the charge-dependent effect of toxin residues weakens as one moves to residues more distant from narrowest part of the channel, defined by the DEKA ring forming the selectivity filter. Fig. 6 B shows that Δφ values at Ala-1529, resulting from charge changes at five different toxin residues, are strongly correlated with the measured fractional residual currents. In the model, μCTX is closer to channel domains I and II, leaving a path on the opposite side, by which ions can bypass the toxin (Fig. 6 C). This conducting bypass is strongly influenced by toxin residue 16; experiments with μCTX-R13Q/K16N showed a strong charge-dependent influence of this residue (see also Fig. 4 C). Consistent with these data, Δφ surfaces predict stronger effects of change in the charge at residue-16 than at 2, 12, and 14 (Table II), thus, providing independent support to coupling studies (Dudley et al., 2000; Li et al., 2001a) regarding the specific toxin orientation and location in the vestibule.

DISCUSSION

μCTX is a potent all-or-none blocker of skeletal muscle sodium channels (Moczydlowski et al., 1986). Block involves the strategic positioning of a positive charge in the ion permeation pathway near, but not at, the selectivity filter. For wild-type toxin, essentially complete block is attained with the basic residue, arginine, at position-13 (Fig. 4 B). Residue-13 is stabilized in the outer vestibule of the pore by multiple toxin–channel binding interactions (Sato et al., 1991; Becker et al., 1992; Dudley et al., 1995; Chahine et al., 1998). Outward rectification found in channels bound by toxin mutants shows that other toxin residues can also impede ion movement (Figs. 2

and 3 A). Also, the observation of a significant I_{res} with all residue-13 mutants, including the bulky R13W (van der Waals volumes [Creighton, 1993] in Å^3: W, 163; R, 148), suggests that probably not even the wild-type toxin completely occludes the selectivity filter. Thus, μCTX block of current appears to rely on electrostatic repulsion of permeating ions centered near residue-13, with supporting contributions from other basic toxin residues (Lys-8, 9, 11, and 16; and Arg-1 and 19).

μCTX residue-13 interacts most prominently with Glu-758, a residue three positions outward along the primary sequence from the channel's selectivity filter (Benitah et al., 1996; Pérez-García et al., 1996; Yamagishi et al., 1997; Chang et al., 1998). In the absence of toxin, Glu-758 is critical for ion conduction but not for selectivity (Terlau et al., 1991; Chiamvimonvat et al., 1996a,b). Mutation of Glu-758 to a cysteine (E758C), which is partially negative at neutral pH, reduces the single-channel current of fenvalerate-activated channels to ~36% of the wild-type value (Chiamvimonvat et al., 1996b), a value between the F_{res}(0 mV) of the R13Q- and R13E-bound channels. Furthermore, cadmium block of these channels results in a residual current ~17.5% of the wild-type channel amplitude (Tsushima et al., 1997), roughly mimicking the block by R13O. The similarity of F_{res} for the E758C channel mutant and that for wild-type channels bound by μCTX mutants suggests that the toxin may block the ionic current through sodium channels in part by reducing the effectiveness of E758 in facilitating cation movement through the pore.

Enhancement of block by increasing residue-13 length appears to reflect a true steric inhibition, rather than a secondary effect of positioning of a side chain charge for effective block, as size dependence is essentially identical for positive, neutral and negative residues. With one exception (alanine), longer amino acids blocked more completely than shorter ones of the same charge (Fig. 3 B). Enhanced block by larger residues may be due to a simple reduction in accessible volume, perhaps supplemented by entropic effects from changes in the degree of ordering of water. Also, deeper intrusion into the channel pore by larger residues may allow them to better interact with Glu-758 and possibly the selectivity filter (Chang et al., 1998). Alternatively, a large residue-13 may be able to displace the flexible E758 side chain (Benitah et al., 1997) out of its normal position in the ion conducting pathway (Chiamvimonvat et al., 1996a,b). This may explain why R13A block did not follow the size trend shown by the other mutants. Block by R13A may result only from the effects of the remaining bulk of the toxin, with the Ala-13 side chain unable to interact either with the conducting ions, or with Glu-758 and other residues lining the permeation pathway. However, Asn-13 in R13N, which gave a slightly larger F_{res}(0 mV) than R13A (Fig. 3 B), may form polar interactions with Glu-758 or other charged or polar channel residues, as is also possible for R13Q and R13W.

In discussing the steric contributions to block, we have, for simplicity, focused on a static view of side chains that occupy a fixed position within the vestibule and reduce the conductance by directly excluding ions from part of the normal conducting pathway. Although this is doubtless an oversimplification, it is consistent with most of the data in hand. At another extreme is the alternate hypothesis that the residue-13 side chain continuously flip-flops, too rapidly to be resolved, between a nonblocking and a fully blocking conformation when the toxin is bound. The magnitude of the residual current would then be determined by the relative flip and flop rates (i.e., it would depend on the stability of the fully blocking configuration). For such an explanation to fit our data, the stability of this blocked configuration would have to be tightly correlated with side chain size. There is no such correlation of residual currents with the affinities determined from the observable blocking kinetics (not shown), which depend strongly on the nature of residue-13. Thus, a simple contribution of steric occlusion to block is a better explanation of the available data.

Use of partially blocking toxin derivatives has opened a unique window into the structural basis of ion conduction. This viewpoint complements and extends studies using site-directed mutagenesis of the channel protein. While one might surmise that binding of the relatively bulky μCTX molecule in the pore might significantly distort pore structure and hence, function, experimental evidence suggests that little general perturbation of pore properties occurs: preliminary experiments under bi-ionic conditions revealed no obvious change in sodium to potassium selectivity (unpublished data); and voltage-dependent activation gating, although measurably shifted on the voltage axis, is modified only subtly (French et al., 1996). Furthermore, binding of R13Q tends to normalize ultraslow inactivation induced by a pore mutation, suggesting that the bound toxin may act as a splint, tending to support the pore in a normal conformation (Todt et al., 1999).

It is of interest to reflect briefly on the molecular strategies of different channel-inhibiting toxins. Imredy and MacKinnon (2000) recently identified residues contributing to the interacting surfaces of δ-dendrotoxin and a voltage-dependent K channel. This toxin appears not to physically occlude the pore, but rather binds to the adjacent "turret" structure; and, although it can induce partial block, the authors argue that this probably results from a conformational restriction of pore dynamics rather than an electrostatic inhibition of conduction. In contrast, as noted earlier, scor-

pion toxins such as charybdotoxin plug potassium channels with a lysine side chain entering the narrow part of the pore (Park and Miller, 1992). Whole-cell data suggest that some pore-targeted peptide calcium channel toxins may cause incomplete block (Mintz, 1994; Sutton et al., 1998). If this is confirmed by detailed single-channel analyses, it may reflect a structural feature common to the vestibules of sodium and calcium channels that is conducive to this behavior. Both competition with guanidinium toxins (Moczydlowski et al., 1986), and transchannel interactions with an ammonium pore blocker (French et al., 1996) suggest that μCTX enters the sodium channel vestibule, but coupling data (Dudley et al., 1995; Chang et al., 1998; Li et al., 2001a,b), and our present results, argue against an intimate interaction with the selectivity filter, and against physical occlusion of the pore. Rather, completeness of block of the current appears to rely on an electrostatic "occlusion." Striking evidence is provided for this conclusion by the strictly empirical, position-dependent correlations between residual current and charge (Fig. 4 B), as well as the model-dependent correlation between residual current and the calculated difference potentials in Fig. 6 B.

Does this strategy have any biological significance for the snail that produces the toxin? A remarkable feature of μCTX action is its isoform specificity: potent inhibition of skeletal muscle channels, but very weak interaction with the highly homologous isoforms in heart and brain. The fish-hunting strategy of certain snails rests on rapid immobilization depending on an initial spastic immobilization initiated by neuronal hyperactivity, followed later by flaccid paralysis that facilitates ingestion (Terlau et al., 1996). In this context, an indiscriminate Na channel-blocking toxin might be less effective than one targeted specifically to skeletal muscle channels, which is distributed via the circulation over a period of seconds to minutes after injection. Evolution of an isoform-specific toxin can be expected to target parts of the channel that are not conserved among related isoforms, and thus not to rely on the selectivity filter for specific binding. For a relatively small toxin like μCTX (22 amino acids as compared with 37 for charybdotoxin, and ~60 for the dendrotoxins), vestibule targeting without intimate binding to the selectivity filter might be more easily achieved.

In conclusion, μCTX blocks sodium channels in at least two ways. Most importantly, the charge of Arg-13 seems, in a highly focal manner, to override the conductance-enhancing electrostatic effects of Glu-758 and other acidic or polar channel residues (e.g., Glu-755; Chang et al., 1998). This appears to be the key requirement for all-or-none block, which is not maintained by charge-conserving substitutions of the smaller basic residues, lysine and ornithine. Second, positive charges at other residues, plus the physical bulk of the toxin, reduce the effective capture volume from which ions enter the channel vestibule.

We thank Drs. Samuel C. Dudley, Jr., Ron Li, Les Tari, and Gerald Zamponi for comments on drafts of the manuscript.

This work was supported by the Canadian Institutes of Health Research (CIHR), the Heart and Stroke Foundation of Alberta, NWT & Nunavut and the National Institutes of Health award RO1 HL65661. R.J. French received salary support as a CIHR Distinguished Scientist and an Alberta Heritage Foundation for Medical Research Medical Scientist.

REFERENCES

Antosiewicz, J., J.A. McCammon, and M.K. Gilson. 1994. Prediction of pH-dependent properties of proteins. *J. Mol. Biol.* 238:415–436.

Becker, S., E. Prusak-Sochaczewski, G. Zamponi, A.G. Beck-Sickinger, R.D. Gordon, and R.J. French. 1992. Action of derivatives of μ-conotoxin GIIIA on sodium channels. Single amino acid substitutions in the toxin separately affect association and dissociation rates. *Biochemistry.* 31:8229–8238.

Benitah, J.-P., G.F. Tomaselli, and E. Marban. 1996. Adjacent pore-lining residues within sodium channels identified by paired cysteine mutagenesis. *Proc. Natl. Acad. Sci. USA.* 93:7392–7396.

Benitah, J.-P., R. Ranjan, T. Yamagishi, M. Janecki, G.F. Tomaselli, and E. Marban. 1997. Molecular motions within the pore of voltage-dependent sodium channels. *Biophys. J.* 73:603–613.

Chahine, M., L.-Q. Chen, N. Fotouhi, R. Walsky, D. Fry, V. Santarelli, R. Horn, and R.G. Kallen. 1995. Characterizing the μ-conotoxin binding site on voltage-sensitive sodium channels with toxin analogs and channel mutations. *Receptors Channels.* 3:161–174.

Chahine, M., J. Sirois, P. Marcotte, L.-Q. Chen, and R.G. Kallen. 1998. Extrapore residues of the S5-S6 loop of domain 2 of the voltage-gated skeletal muscle sodium channel (rSkM1) contribute to the μ-conotoxin GIIIA binding site. *Biophys. J.* 75:236–246.

Chang, N.S., R.J. French, G.M. Lipkind, H.A. Fozzard, and S. Dudley, Jr. 1998. Predominant interactions between μ-conotoxin Arg-13 and the skeletal muscle Na^+ channel localized by mutant cycle analysis. *Biochemistry.* 37:4407–4419.

Chiamvimonvat, N., M.T. Pérez-Garcia, R. Ranjan, E. Marban, and G.F. Tomaselli. 1996a. Depth asymmetries of the pore-lining segments of the Na^+ channel revealed by cysteine mutagenesis. *Neuron.* 16:1037–1047.

Chiamvimonvat, N., M.T. Pérez-García, G.F. Tomaselli, and E. Marban. 1996b. Control of ion flux and selectivity by negatively charged residues in the outer mouth of rat sodium channels. *J. Physiol.* 491.1:51–59.

Creighton, T.E. 1993. Chemical properties of polypeptides. *In* Proteins: Structures and Molecular Properties. W.H. Freeman and Company. 1–47.

Cruz, L.J., W.R. Gray, B.M. Olivera, R.D. Zeikus, L. Kerr, D. Yoshikami, and E. Moczydlowski. 1985. *Conus geographus* toxins that discriminate between neuronal and muscle sodium channels. *J. Biol. Chem.* 260:9280–9288.

Doyle, D.A., J.M. Cabral, R.A. Pfuetzner, A. Kuo, J.M. Gulbis, S.L. Cohen, B.T. Chait, and R. MacKinnon. 1998. The structure of the potassium channel: molecular basis of K^+ conduction and selectivity. *Science.* 280:69–77.

Dudley, S.C., H. Todt, G. Lipkind, and H.A. Fozzard. 1995. A μ-conotoxin-insensitive Na^+ channel mutant: possible localization of a binding site at the outer vestibule. *Biophys. J.* 69:1657–1665.

Dudley, S.C., Jr., N. Chang, J. Hall, G. Lipkind, H.A. Fozzard, and R.J. French. 2000. μ-Conotoxin interactions with the voltage-gated Na^+ channel predict a clockwise arrangement of domains.

J. Gen. Physiol. 116:679–689.

French, R.J., and R. Horn. 1997. Shifts of macroscopic current activation in partially blocked sodium channels. Interaction between the voltage sensor and a μ-conotoxin. *In* From Ion Channels to Cell-to-Cell Conversations. R. Latorre and J.C. Sáez, editors. Plenum Press, New York. 67–89.

French, R.J., E. Prusak-Sochaczewski, G.W. Zamponi, S. Becker, A.S. Kularatna, and R. Horn. 1996. Interactions between a pore-blocking peptide and the voltage sensor of the sodium channel: an electrostatic approach to channel geometry. *Neuron.* 16:407–413.

Gilson, M.K., and B.H. Honig. 1987. Calculation of electrostatic potentials in an enzyme active site. *Nature.* 330:84–86.

Gray, W.R., B.M. Olivera, and L.J. Cruz. 1988. Peptide toxins from venomous *Conus* snails. *Annu. Rev. Biochem.* 57:665–700.

Hille, B. 1992. Ionic Channels of Excitable Membranes. 2nd ed. Sinauer Associates. Inc., Sunderland, MA. 607 pp.

Imredy, J.P., and R. MacKinnon. 2000. Energetic and structural interactions between delta-dendrotoxin and a voltage-gated potassium channel. *J. Mol. Biol.* 296:1283–1294.

Kaerner, A., and D.L. Rabenstein. 1999. Stability and structure-forming properties of the two disulfide bonds of α-conotoxin GI. *Biochemisty.* 38:5459–5470.

Khodorov, B.I. 1985. Batrachotoxin as a tool to study voltage-sensitive sodium channels of excitable membranes. *Prog. Biophys. Mol. Biol.* 45:57–148.

Lancelin, J.-M., D. Kohda, S.-I. Tate, Y. Yanagawa, T. Abe, M. Satake, and F. Inagaki. 1991. Tertiary structure of conotoxin GIIIA in aqueous solution. *Biochemistry.* 30:6908–6916.

Li, R.A., I.L. Ennis, R.J. French, S.C. Dudley, Jr., G.F. Tomaselli, and E. Marbán. 2001a. Clockwise domain arrangement of the sodium channel revealed by μ-conotoxin (GIIIA) docking orientation. *J. Biol. Chem.* 276:11072–11077.

Li, R.A., I.L. Ennis, G.F. Tomaselli, R.J. French, and E. Marbán. 2001b. Latent specificity of molecular recognition in sodium channels engineered to discriminate between two "indistinguishable" μ-conotoxins. *Biochemistry.* 40:6002–6008.

Lipkind, G.M., and H.A. Fozzard. 1994. A structural model of the tetrodotoxin and saxitoxin binding site of the Na^+ channel. *Biophys. J.* 66:1–13.

Lipkind, G.M., and H.A. Fozzard. 2000. KcsA crystal structure as framework for a molecular model for the Na^+ channel pore. *Biochemistry.* 39:8161–8170.

MacKinnon, R., S.L. Cohen, A. Kuo, A. Lee, and B.T. Chait. 1998. Structural conservation in prokaryotic and eukaryotic potassium channels. *Science.* 280:106–109.

Miller, C. 1995. The charybdotoxin family of K^+ channel-blocking peptides. *Neuron.* 15:5–10.

Mintz, I.M. 1994. Block of Ca channels in rat central neurons by the spider toxin ω-Aga-IIIA. *J. Neurosci.* 14:2844–2853.

Moczydlowski, E., B.M. Olivera, W.R. Gray, and G.R. Strichartz. 1986. Discrimination of muscle and neuronal Na-channel subtypes by binding competition between [^{3}H]saxitoxin and μ-conotoxins. *Proc. Natl. Acad. Sci. USA.* 83:5321–5325.

Park, C.-S., and C. Miller. 1992. Interaction of charybdotoxin with permeant ions inside the pore of a K^+ channel. *Neuron.* 9:307–313.

Pérez-García, M.T., N. Chiamvimonvat, E. Marban, and G.F. Tomaselli. 1996. Structure of the sodium channel pore revealed by serial cysteine mutagenesis. *Proc. Natl. Acad. Sci. USA.* 93:300–304.

Price-Carter, M., M.S. Hull, and D.P. Goldenberg. 1998. Roles of individual disulfide bonds in the stability and folding of an omega-conotoxin. *Biochemistry.* 37:9851–9861.

Ravindran, A., H. Kwiecinski, O. Alvarez, G. Eisenman, and E. Moczydlowski. 1992. Modeling ion permeation through batrachotoxin-modified Na^+ channels from rat skeletal muscle with a multi-ion pore. *Biophys. J.* 61:494–508.

Sato, K., Y. Ishida, K. Wakamatsu, R. Kato, H. Honda, H. Nakamura, M. Ohya, D. Kohda, F. Inagaki, J.-M. Lancelin, and Y. Ohizumi. 1991. Active site of μ-conotoxin GIIIA, a peptide blocker of muscle sodium channels. *J. Biol. Chem.* 266:16989–16991.

Sharp, K.A., and B. Honig. 1990. Electrostatic interactions in macromolecules: theory and applications. *Annu. Rev. Biophys. Chem.* 19:301–332.

Sutton, K.G., C. Siok, A. Stea, G.W. Zamponi, S.D. Heck, R.A. Volkmann, M.K. Ahlijanian, and T.P. Snutch. 1998. Inhibition of neuronal calcium channels by a novel peptide spider toxin, DW13.3. *Mol. Pharmacol.* 54:407–418.

Terlau, H., S.H. Heinemann, W. Stühmer, M. Pusch, F. Conti, K. Imoto, and S. Numa. 1991. Mapping the site of block by tetrodotoxin and saxitoxin of sodium channel II. *FEBS Letters.* 293:93–96.

Terlau, H., K.-J. Shon, M. Grilley, M. Stocker, W. Stühmer, and B.M. Olivera. 1996. Strategy for rapid immobilization of prey by a fish-hunting marine snail. *Nature.* 381:148–151.

Todt, H., S.C. Dudley, Jr., J.W. Kyle, R.J. French, and H.A. Fozzard. 1999. Ultra-slow inactivation in μ1 Na^+ channels is produced by a structural rearrangement of the outer vestibule. *Biophys. J.* 76: 1333–1345.

Tsushima, R.G., R.A. Li, and P.H. Backx. 1997. P-loop flexibility in Na^+ channel pores revealed by single- and double-cysteine replacements. *J. Gen. Physiol.* 110:59–72.

Wakamatsu, K., D. Kohda, H. Hatanaka, J.-M. Lancelin, Y. Ishida, M. Oya, H. Nakamura, F. Inagaki, and K. Sato. 1992. Structure-activity relationships of μ-conotoxin GIIIA: structure determination of active and inactive sodium channel blocker peptides by NMR and simulated annealing calculations. *Biochemistry.* 31:12577–12584.

Yamagishi, T., M. Janecki, E. Marban, and G.F. Tomaselli. 1997. Topology of the P segments in the sodium channel pore revealed by cysteine mutagenesis. *Biophys. J.* 73:195–204.